

# Machine Learning-Based Enhancements of Empirical Energy Functions: Structure, Dynamics and Spectroscopy of Modified Benzenes

Kham Lek Chaton<sup>†</sup> and Markus Meuwly<sup>\*,†,‡</sup>

<sup>†</sup>*Department of Chemistry, University of Basel, Klingelbergstrasse 80, CH-4056 Basel, Switzerland.*

<sup>‡</sup>*Department of Chemistry, Brown University, USA*

E-mail: m.meuwly@unibas.ch

November 14, 2024

## Abstract

The effect of replacing individual contributions to an empirical energy function are assessed for halogenated benzenes (X-Bz, X = H, F, Cl, Br) and chlorinated phenols (Cl-PhOH). Introducing electrostatic models based on distributed charges (MDCM) instead of usual atom-centered point charges yields overestimated hydration free energies unless the van der Waals parameters are reparametrized. Scaling van der Waals ranges by 10 % to 20 % for three Cl-PhOH and most X-Bz yield results within experimental error bars, which is encouraging, whereas for benzene (H-Bz) point charge-based models are sufficient. Replacing the bonded terms by a neural network-trained energy function with either fluctuating charges or MDCM electrostatics also yields qualitatively correct hydration free energies which still require adaptation of the van der Waals parameters. The infrared spectroscopy of Cl-PhOH is rather well predicted by all models although

the ML-based energy function performs somewhat better in the region of the framework modes. It is concluded that refinements of empirical energy functions for targeted applications is a meaningful way towards more quantitative simulations.

## 1 Introduction

The success of empirical energy functions rests on two ingredients: i) their functional dependence is sufficiently simple to allow rapid evaluation for stable and long-time ( $\mu\text{s}$  or longer) simulations of large systems ( $10^6$  atoms or larger) and ii) their acceptable accuracy in modelling intra- and intermolecular interactions which allows qualitative or semi-quantitative molecular-level studies, depending on the observable(s) considered and the agreement with experiments sought. While existing force fields exploit new hardware to simulate ever larger systems and longer timescales,<sup>1</sup> increased computational power also provides an opportunity to include more detail to refine force fields that are still applicable to systems and timescales of chemical or biochemical interest. Crucial to this task is determining to what extent increasing the detail of each term provides greater accuracy in describing the intermolecular interactions.<sup>2</sup> At the same time, the final model needs to be widely applicable with the possibility to parametrize it even for highly heterogeneous chemical systems, such as ionic liquids.<sup>3,4</sup>

Empirical energy functions have a long and successful history as exemplified by the widely used parametrizations are the CHARMM,<sup>5</sup> Amber,<sup>6</sup> Gromos,<sup>7</sup> and OPLS<sup>8</sup> energy functions. Such energy functions were and are being successfully applied to study proteins,<sup>9</sup> nucleic acids,<sup>10</sup> organic crystals,<sup>11</sup> or materials,<sup>12</sup> to name only a few applications. One of the broadly applicable empirical energy functions is the CGenFF parametrization which is the CHARMM General Force Field.<sup>13,14</sup> This energy function is available as an additive and a polarizable variant using the Drude-oscillator approach.

On the other hand, most terms in an empirical energy function are first-order approximations to more physically meaningful terms. One example concerns harmonic, quadratic terms for chemical bonds which are suitable to describe equilibrium structures of molecules and small-amplitude vibrations within a normal mode approximation. However, for anharmonic vibrations one needs to go beyond such an approximation and include higher-order terms (cubic, quartic) such as done, e.g., in the Merck Molecular Force Field (MMFF).<sup>15</sup> There are alternative possibilities such as replacing the harmonic terms by Morse-oscillators or machine-learned energy functions using reproducing kernels or neural networks.<sup>16-19</sup> For studying the infrared spectroscopy of small molecules in heterogeneous environments and comparing with experiments to provide interpretations and understanding, the simplest parametrizations are clearly insufficient.<sup>20,21</sup> Similarly, to characterize energy flow in molecules, the coupling between different internal degrees of freedom needs to be captured considerably more precisely for meaningful analysis and potentially predictive simulations.<sup>22,23</sup> In all these cases, replacing specific terms in the empirical energy functions by more appropriate functional forms will enhance the performance and improve the quality of the simulations carried out with these energy functions.

Along similar lines, atom-centered point charges as an approximation to the more general multipolar expansion of electrostatic interactions can be replaced by, for example, extended charge models,<sup>24-28</sup> atom-centered multipoles,<sup>29-33</sup> or off-centered distributed point charges.<sup>34-39</sup> Such more elaborate models for the electrostatics capture the anisotropy of the charge distribution around a particular interaction site. This is, for example, relevant when representing lone pairs as for water or  $\sigma$ -holes for halogenated compounds.<sup>40,41</sup> It is also possible to yet include changes in the electrostatics as the structure of a molecule changes along a MD trajectory. Such “fluctuating charges” or “fluctuating multipoles” are also capable of encapsulating bond polarization<sup>37,38,42-46</sup> or qualitatively describing charge reorganization for bond breaking and bond-formation.<sup>47</sup>

The present work explores the effects of replacing bonded and electrostatic interactions in the CGenFF empirical energy functions for halogenated benzenes and Chloro-phenol with the chloride atom at its *o*-, *p*-, and *m*-positions relative to the hydroxyl. First, the computational methods are presented, followed by structural, spectroscopic and thermodynamic properties.

## 2 Methods

### 2.1 Atomistic Simulations

All simulations were performed using CHARMM.<sup>48,49</sup> The off-centered minimal distributed charge model MDCM were handled through the DCM<sup>34,35</sup> module in CHARMM, and the PhysNet-trained PES<sup>50</sup> was run through pyCHARMM.<sup>51,52</sup>

Simulations for all solutes were carried out in a  $32^3 \text{ \AA}^3$  cubic water box using the TIP3P<sup>53</sup> water model. There were a total of 1695 and 1696 atoms for the Halobenzene (X-Bz) and fluoro-substituted phenol (F-PhOH) systems, respectively. The systems were initially minimized using 500 steps of Steepest Descent (SD) followed by 1000 steps of Adopted Basis Newton-Raphson (ABNR) minimization. Subsequently, a heating and equilibration step in the *NVT* ensemble for 125 ps with timestep of  $\Delta t = 1$  fs was employed. The Nose-Hoover thermostat was used to maintain the temperature around 303.15 K. This was followed by 1 ns production simulations in the *NPT* ensemble using the Leapfrog Verlet integrator with a timestep of  $\Delta t = 0.2$  fs because bonds involving the solute hydrogen atoms were allowed to change. The pressure was controlled using the Langevin Piston barostat with a reference pressure of 1 atm and SHAKE<sup>54</sup> was used to constrain bonds involving hydrogen atoms in water. Long range interactions were treated using particle Ewald mesh PME with a cutoff of

16 Å and the Lennard-Jones interactions were switched between 10 Å and 12 Å. For analysis, every tenth snapshot was saved.

## 2.2 Intermolecular Interactions

The present work uses and evaluates different representations of the bonded and electrostatic interactions. For one, the CGenFF<sup>13,14</sup> parametrization, consistent with the TIP3P water model was used for all solutes. Secondly, the ESP of the solutes was used to obtain off-centered, minimal distributed charges (MDCM).<sup>35</sup> Thirdly, the total energy function of the solutes was represented as a machine-learned PES using the PhysNet<sup>50</sup> neural network architecture. Such a representation replaces all terms from an empirical energy function except for the van der Waals terms for which initially those from the CGenFF parametrization were used. Finally, the fourth energy function combined the PhysNet representation whereby the atom-centered fluctuating charges from PhysNet were replaced by the off-centered MDCM charges.

To improve the representation of the electrostatic potential (ESP) around a molecule beyond that provided by atom-centered point charges, models using off-centered charges or multipole moments have been devised.<sup>25,29,30</sup> Alternatively, point-charge based models such as the distributed charge model (DCM) or minimal DCMs (MDCM) were developed and tested.<sup>34,35</sup> Such models are based on the notion that every higher-order multipole can be replaced by closely spaced point charges around an interaction site. For example, an atomic dipole moment corresponds to a closely spaced pair of one positive and one negative charge.

The reference ESP from electronic structure calculations was obtained on a grid of  $M$  reference points  $(x_m, y_m, z_m)$ ,  $m = 1 \dots M$  from the electron density of the converged wavefunction using the cubegen utility.<sup>55</sup> This reference ESP was represented as a minimal DCM model

(MDCM) using  $N$  off-center charges fitted to reproduce the reference ESP with root mean squared error  $\text{RMSE}_N$  using differential evolution.<sup>34-36,56</sup> Initially, models with  $N_1 \leq N \leq N_2$  MDCM charges were generated. The lowest  $\text{RMSE}_N$  for each value of  $N$  is recorded. If  $\text{RMSE}_N$  is constant for the largest values of  $N = [N_2, \dots, N_2 - 3]$  the model with the lowest  $\text{RMSE}_N$  is used. Otherwise,  $N$  was further increased and DE was repeated until the  $\text{RMSE}_N$  converged to within 1 kcal/mol.

## 2.3 Intramolecular Interactions

For the bonded terms, a PhysNet model was trained to best describe the total energy of each molecule as a function of geometry.<sup>50</sup> PhysNet is a message passing NN<sup>57</sup> that falls under the family of graph neural network.<sup>58</sup> Using energies, forces and dipole moments for  $N$  training structures, the loss function

$$\begin{aligned} \mathcal{L} = & w_E |E - E^{\text{ref}}| + \frac{w_F}{3N} \sum_{i=1}^N \sum_{\alpha=1}^3 \left| -\frac{\partial E}{\partial r_{i,\alpha}} - F_{i,\alpha}^{\text{ref}} \right| \\ & + w_Q \left| \sum_{i=1}^N q_i - Q^{\text{ref}} \right| + \frac{w_p}{3} \sum_{\alpha=1}^3 \left| \sum_{i=1}^N q_i r_{i,\alpha} - p_\alpha^{\text{ref}} \right| + \mathcal{L}_{\text{nh}}. \end{aligned} \quad (1)$$

was minimized using the Adam optimizer.<sup>59,60</sup> Here,  $E^{\text{ref}}$ ,  $F_{i,\alpha}^{\text{ref}}$ ,  $Q^{\text{ref}}$ , and  $p_\alpha^{\text{ref}}$  are the reference energies, the Cartesian components of the force on each atom  $i$ , the total charge, and the Cartesian components of the reference dipole moment respectively. The hyperparameters<sup>50,51</sup>  $w_i$   $i \in \{E, F, Q, p\}$  differentially weigh the contributions of the loss function and were  $w_E = 1$ ,  $w_F \sim 52.92$ ,  $w_Q \sim 14.39$  and  $w_p \sim 27.21$ , respectively. Finally, the term  $\mathcal{L}_{\text{nh}}$  is a ‘‘nonhierarchical penalty’’ that serves as a regularization to the loss function.<sup>50</sup> In the following the PhysNet representations were used in two ways. The first employed the full model that comprises representations of the bonded terms and fluctuating point charges whereas for the second usage the fluctuating point charges were replaced by the MDCM

models.

Reference data for the initial training were generated from MD simulations using semi-empirical tight binding GFN2-xTB<sup>61</sup> at temperatures  $T \in 100, 300, 1000, 1500, 2000$  K using ASE.<sup>62</sup> From simulations at each temperature,  $\sim 5000$  structures were extracted. Therefore a total of 25000 geometries was obtained. For each geometry a single point calculation was carried out at the MP2/6-31G(d,p) level of theory using MOLPRO2020.<sup>63</sup>

The datasets for the X-Benzenes (X = H, F, Cl, Br) were generated following a comparable procedure. However, two additional sets of geometries were generated (at 200 K and 2500 K). Therefore, a total of 35000 structures was generated from MD simulations using the semiempirical GFN2-xTB model.<sup>61</sup> For each geometry a single point calculation was carried out at the MP2/6-31G(d,p) level of theory using MOLPRO2020.<sup>63</sup> Therefore, for all the X-Benzenes (X = H, F, Cl, Br) the total data set contained  $\sim 35000$  structures, energies and forces.

Reference ESPs for all compounds considered were calculated using Gaussian16 and the cubegen facility.<sup>55</sup> The data for the X-Benzenes (where X= H, F, Cl, Br) was calculated at the PBE1PBE/aug-cc-pvdz level of theory and for the three Cl-PhOH they were calculated at the MP2/aug-cc-pVTZ level of theory because PBE1PBE/aug-cc-pvdz calculations did not give any discernible sigma hole.

## 2.4 Analysis and Observables

The radial distribution function  $g(r)$  and infrared spectra  $I(\omega)$  were obtained from MD simulations of the hydrated compounds. All distribution functions  $g(r)$  were calculated using MDAnalysis.<sup>64,65</sup> To obtain the infrared spectrum  $I(\omega)$ , the dipole moment time series

$\vec{\mu}(t)$  of the solute was computed from the simulations. For MD using the CGenFF force field,  $\vec{\mu}(t)$  was also obtained from MDAnalysis<sup>64,65</sup> whereas for the other three energy functions (MDCM, PhysNet and PhysNet+MDCM),  $\vec{\mu}(t)$  was obtained from CHARMM and pyCHARMM, respectively.

From the dipole moment time series  $\vec{\mu}(t)$ , the autocorrelation function,  $C_\mu(t) = \langle \text{vec}\mu(0)\vec{\mu}(t) \rangle$  was calculated. Fourier transformation of  $C_\mu(t)$  using a Blackman window yields the infrared spectrum

$$I(\omega) = \int e^{-i\omega t} C_\mu(t) dt \quad (2)$$

which was multiplied by a quantum correction factor  $(1 - e^{-\beta\hbar\omega})$  to obtain the final signal.<sup>66</sup> Here,  $\beta = \frac{1}{k_B T}$ ,  $k_B$  is the Boltzmann constant,  $T$  is the temperature in K, and  $\hbar$  is the reduced Planck constant.

Hydration free energies  $\Delta G_{\text{hyd}}$  for all compounds in water were computed from thermodynamic integration.<sup>67,68</sup> For this, the solute was sampled in the gas phase and in pure water. The condensed-phase simulations were carried out in the  $NpT$  ensemble with 1683 water molecules, see above. Simulations with 24 different coupling parameters  $\lambda \in (0, 1)$  for electrostatic and vdW interactions were carried out, respectively. Initial conditions for these simulation were taken from an unbiased simulation, equilibrated for 50 ps with the respective coupling parameter  $\lambda$  and run for another 200 ps for statistical sampling. The total hydration free energy was then accumulated from

$$\Delta G_{\text{hyd}} = \sum_{\lambda} [(H_{\text{solv}}^{\text{elec}}(\lambda) - H_{\text{gas}}^{\text{elec}}(\lambda)) + (H_{\text{solv}}^{\text{vdW}}(\lambda) - H_{\text{gas}}^{\text{vdW}}(\lambda))] \Delta\lambda \quad (3)$$

## 3 Results

### 3.1 Validation of the PhysNet Models

The trained PhysNet models were validated with respect to energy, forces and Normal mode analysis. The performance for the Cl-PhOHs is reported in Figure 1. Among the 3 molecules, *p*-chlorophenol had the highest mean absolute MAE( $E$ ) error with 0.10 kcal/mol and 0.07 kcal/mol in test ( $\sim 5000$  structures) and training sets, respectively. The largest RMSE( $E$ ) also occurred for *p*-chlorophenol which were 0.37 kcal/mol and 0.08 kcal/mol in test and training sets. Compared to this, the maximum absolute error mAE( $E$ ) in the test and training sets were 4.86 kcal/mol and 0.38 kcal/mol for *o*-Cl-PhOH and *m*-Cl-PhOH, respectively. The reported energetics spanned over a range of 250 kcal/mol and performed within acceptable range of errors except for a few outliers at higher energies which correspond to more pronounced molecular distortions. In terms of forces the highest MAE( $F$ ) in the test and training sets were recorded for *o*-Cl-PhOH with 0.39 kcal/mol/Å and 0.02 kcal/mol/Å, respectively. This is consistent for RMSE as well with,  $\sim 0.03$  kcal/mol/Å and 1.05 kcal/mol/Å for the test and training sets. The reported ranges of errors for the Halobenzene are comparable and consistent with earlier work on similar compounds<sup>51</sup> which further validates the present ML-PESs.

Another validation of the PESs is afforded by considering the normal mode frequencies. The average difference between all reference *ab initio* and predicted normal mode frequencies for Cl-PhOH was  $\Delta\omega \sim \pm 5$  cm<sup>-1</sup> with a maximum error of  $\Delta\omega \sim 20$  cm<sup>-1</sup>, see Figure S2. This is a significant improvement over an earlier study<sup>51</sup> for which the maximum  $\Delta\omega$  was  $\sim \pm 100$  cm<sup>-1</sup>. The improvement can be attributed to including a larger number of near-equilibrium structures from MD sampling at 200 K, 300 K, and 1000 K. On the other hand, for the X-Bz, see Figure 2, the maximum error is  $\Delta\omega \sim 50$  cm<sup>-1</sup> whereas on average, again,  $\Delta\omega \sim \pm 5$  cm<sup>-1</sup>. For both species, see Figures S2 and 2, an increase in  $\Delta\omega$  for the lower frequency

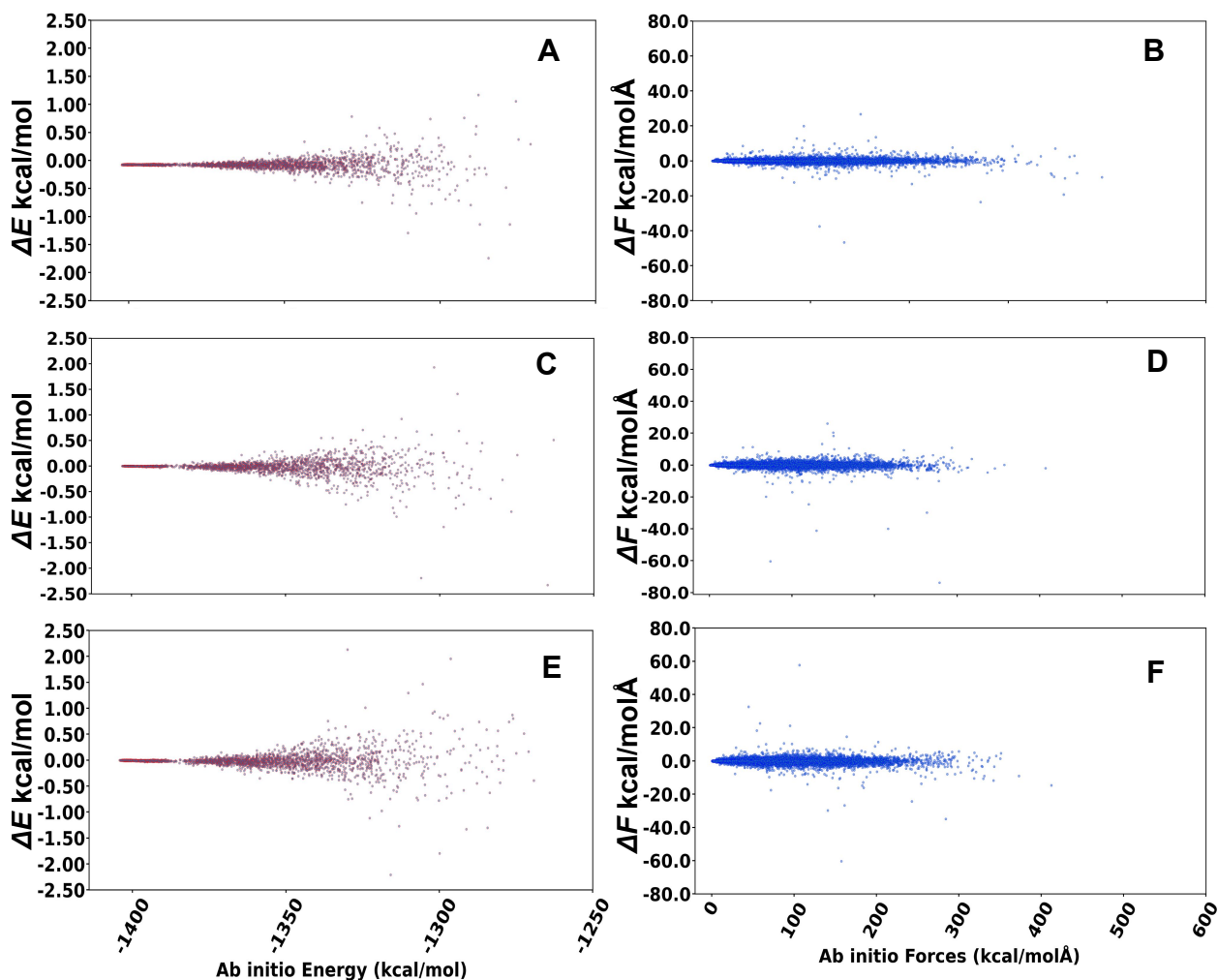


Figure 1: Comparison of PhysNet prediction for the test set (2500 structures) against reference MP2/6-31G(d,p) energies and forces for *p*-Cl-PhOH (panels A, B), *m*-Cl-PhOH (C, D), and *o*-Cl-PhOH (E, F). Left and right hand columns are for energies and the magnitude of the forces, respectively.

ranges was observed. The motion for which the difference between reference and model harmonic frequency is largest is the ring out-of-plane bending mode, see Figure 2 which was also the outlier in previous studies. However, despite including additional samples along this normal mode in the training the deviations persisted.

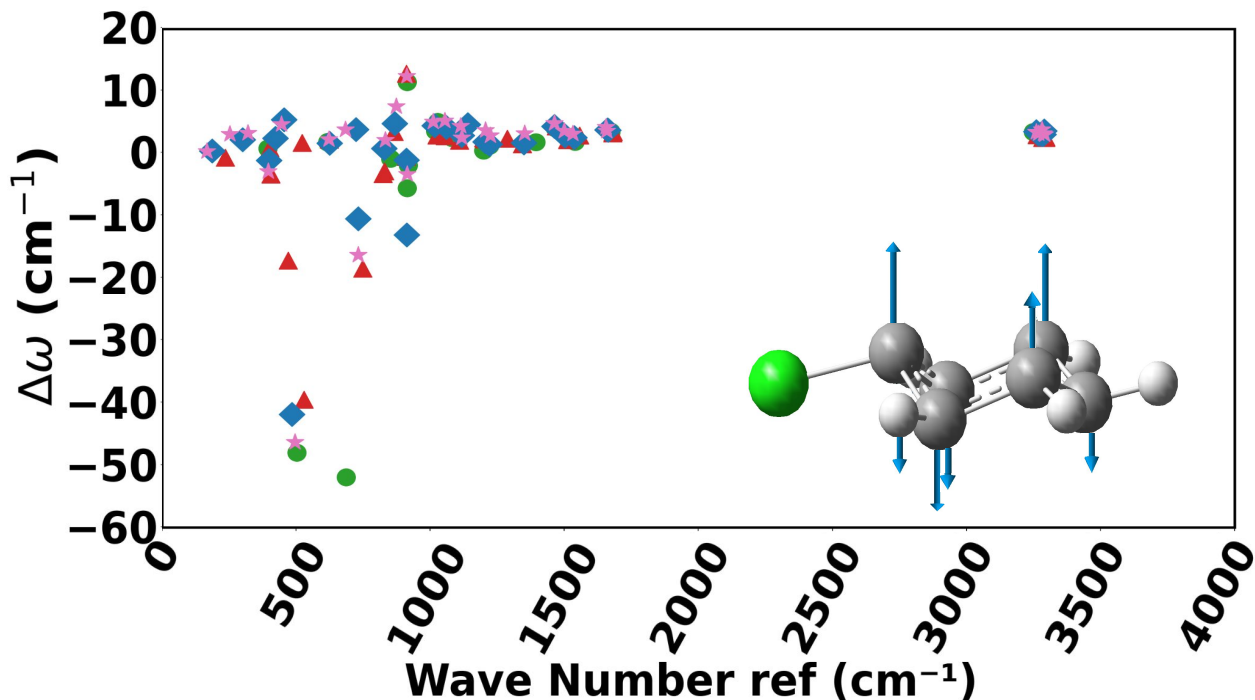


Figure 2: Normal mode analysis for X-Bz (where X = H, F, Cl, Br). Depending on the frequency  $\omega$  of the normal mode the difference between *ab initio* and harmonic frequencies from PhysNet,  $\Delta\omega$ , differs. The molecular structure shown is Cl-Bz and the normal mode vector is that with the maximum deviation  $\Delta\omega$ . Circles, triangles, diamonds, and stars are for H-Bz, F-Bz, Cl-Bz, and Br-Bz, respectively.

### 3.2 Quality of the MDCM Electrostatic Models

The differences between the *ab initio* reference ESP and that from the MDCM models are reported in the left hand columns in Figures 3 and 4 for the four X-Bz and the three Cl-PhOH, respectively. The right hand columns report the positions of the conformationally averaged charge positions together with the ESP generated by the MDCM models. In Figure 3 the  $\sigma$ -hole (blue density along the C-X axis) on the X-site (X = H, F, Cl, Br) grows as the size of the halogen atom increases. It is also found that the negative density around the C-X bond grows in magnitude in going from F to Br. The average total errors range from 0.70 to 0.48 kcal/mol in going from H-Bz to Br-Bz using 19 MDCM charges. This is consistent with earlier work that reported an error 0.35 kcal/mol for Br-Bz for which, however, the density was determined at the B97D3/aug-cc-pVTZ level of theory.<sup>35</sup> Also, the decreasing error in

going from the close to the long range agrees with earlier work. Overall, the performance of the 19-charge MDCM models for X-Bz is satisfactory.

Table 1: Quality of the MDCM models for X-Bz and *p*-, *m*-, *o*-Cl-PhOH. RMSE and maximum errors (in brackets) in (kcal/mol)/*e* for each model are reported.  $N_{\text{MDCM}}$  is the total number of MDCM charges. Close, mid, and long range correspond to the ESP in regions within  $1.6\sigma$ , between  $1.6\sigma$  and  $2.2\sigma$ , and beyond  $2.2\sigma$  away from the nuclei where  $\sigma$  are the van der Waals radii of the respective atoms.<sup>69</sup>

Molecule	$N_{\text{MDCM}}$	Errors ( $\text{ESP}_{\text{ref}} - \text{ESP}_{\text{MDCM}}$ ) kcal/mol			
		Close range	Mid range	Long range	Total
H-Bz	19	1.43 (7.37)	0.44 (2.18)	0.15 (0.83)	0.70 (7.37)
F-Bz	19	1.26 (10.22)	0.32 (1.44)	0.11 (0.59)	0.62 (10.23)
Cl-Bz	19	1.24 (7.18)	0.34 (2.09)	0.12 (0.92)	0.52 (7.18)
Br-Bz	19	1.35 (7.10)	0.36 (2.34)	0.12 (1.02)	0.48 (7.10)
<i>p</i> -Cl-PhOH	35	2.37 (13.49)	1.79 (4.52)	1.36 (2.62)	1.67 (13.49)
<i>m</i> -Cl-PhOH	36	1.80 (8.92)	0.79 (3.29)	0.41 (1.56)	0.86 (8.92)
<i>o</i> -Cl-PhOH	34	2.13 (12.9)	0.77 (3.21)	0.34 (1.16)	0.96 (12.90)

For the three Cl-PhOH substitutions (*o*-, *m*-, and *p*-Cl-PhOH) the reference and MDCM-based ESPs are compared in Figure 4 (left hand column) for one of the structures used for obtaining the conformationally averaged MDCM models. The right-hand column clearly display the  $\sigma$ -holes from the MDCM models for *p*- and *m*-Cl-PhOH as regions of positive charge density along the C-Cl axis whereas for *o*-Cl-PhOH the  $\sigma$ -hole is not particularly pronounced. This may be caused by the proximity of the -OH group. It is interesting to note that the centered negative charge distribution around the -OH group for *p*- and *m*-Cl-PhOH is shifted away from the halogenated site for *o*-Cl-PhOH. This leads to a  $\sigma$ -hole for *o*-Cl-PhOH that is moved away from the C-Cl axis. The total errors for different regions away from the molecule (close, mid, long range and total) are summarized in Table 1. The overall performance of the MDCM models is around 1 kcal/mol on average except for *p*-Cl-PhOH for which the error is 1.6 kcal/mol. Compared with X-Bz the average errors

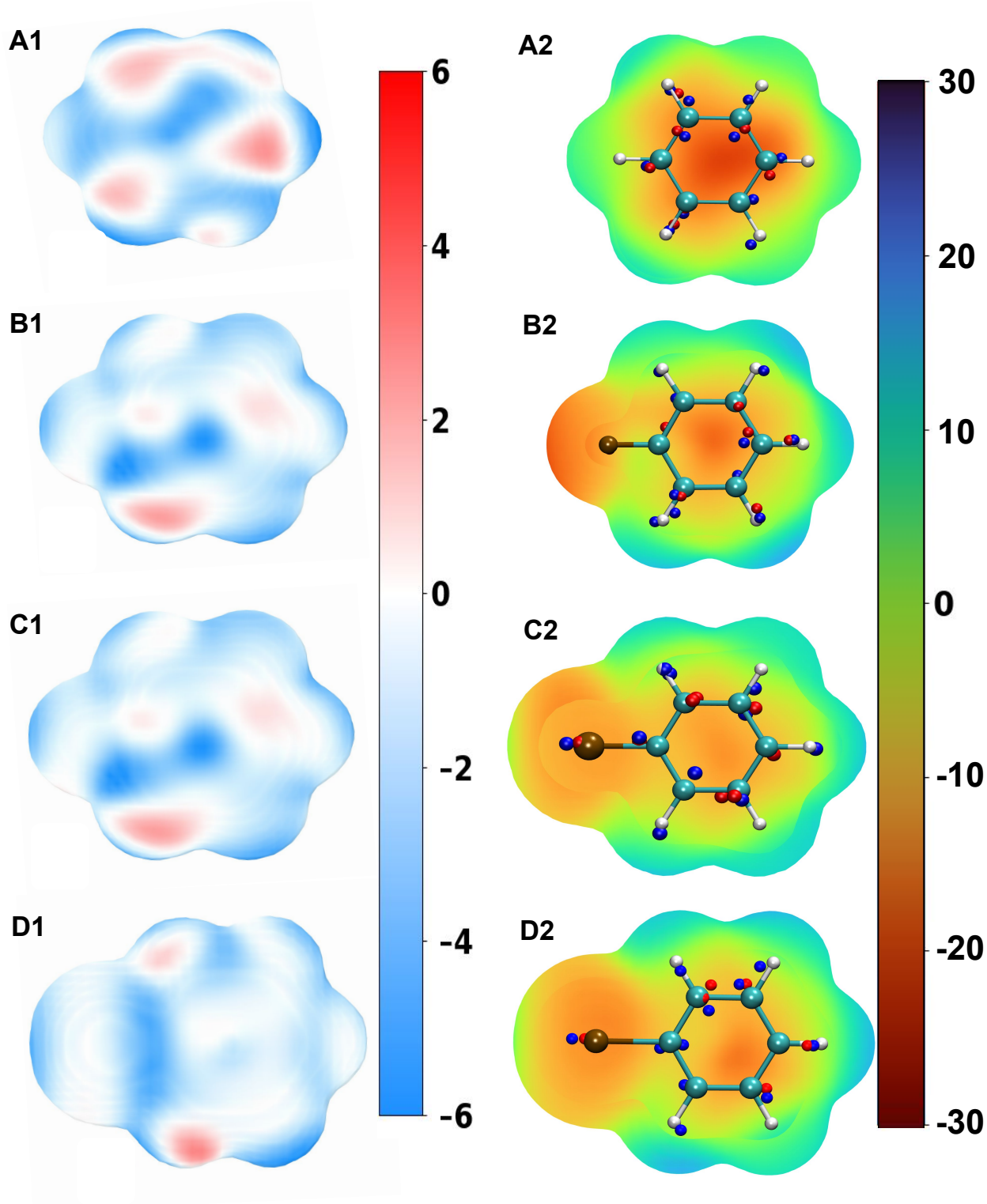


Figure 3: Difference ESP ( $\Delta\text{ESP}$ ) between the reference (PBE1PBE/aug-cc-pvdz) and MDCM-generated ESP (left column) and the ESP from the MDCM models (right column) for X-Bz ( $X = \text{H}, \text{F}, \text{Cl}, \text{Br}$  from top to bottom) on the 0.001 isosurface. In panels A2 to D2 the positions of the positive and negative MDCM charges are reported as small blue and red spheres. The geometries are the respective equilibrium structures at the PBE1PBE/aug-cc-pvdz level. The average errors for the close, mid, and long ranges are reported in Table 1.

are about a factor of two larger for the three Cl-PhOH. Further reduction of the errors may be achieved by using a flexible or kernelized MDCM model.<sup>37,38</sup>

### 3.3 Structural Dynamics in Solution

Using the PhysNet and MDCM models the structural dynamics in solution was investigated next. Simulations were carried out using the 4 different energy functions: conventional CGenFF (using point charges), CGenFF but point charges replaced by the MDCM models, PhysNet, and PhysNet+MDCM where the fluctuating PhysNet charges are replaced by MDCM charges. All these simulations were carried out using conventional CHARMM (CGenFF, MDCM) or pyCHARMM with provisions for ML-PESs (PhysNet and PhysNet+MDCM).<sup>48-52</sup> The van der Waals parameters in all four cases were those from the CGenFF force field.

The structural dynamics of the hydrated X-Bz and Cl-PhOH solutes were characterized in terms of pair distribution functions  $g(r)$  between solute and solvent. For X-Bz ( $X = \text{F}, \text{Cl}, \text{Br}$ ) the  $g_{\text{X-O}_w}(r)$  between the halogen and the water-oxygen atoms are shown in Figure 5 using the different energy functions (CGenFF, MDCM, PhysNet and PhysNet+MDCM). For F-Bz (Figure 5A) the occupation in the first solvent shell is  $\sim 25\%$  larger from the simulations using the MDCM model together with either CGenFF bonded parameters or PhysNet. The CGenFF and PhysNet simulations using atom-centered point charges (fixed vs. fluctuating) yield comparable  $g(r)$ . For Cl-Bz, all four models give essentially identical radial distribution functions whereas for Br-Bz the observations are similar to F-Bz. It is noted that for X-O<sub>w</sub> separations larger than 5 Å the MDCM models feature some overstructuring which is not present in the atom-centered point charge models. Such overstructuring is also known from simulations using atom-centered multipoles.<sup>3</sup>

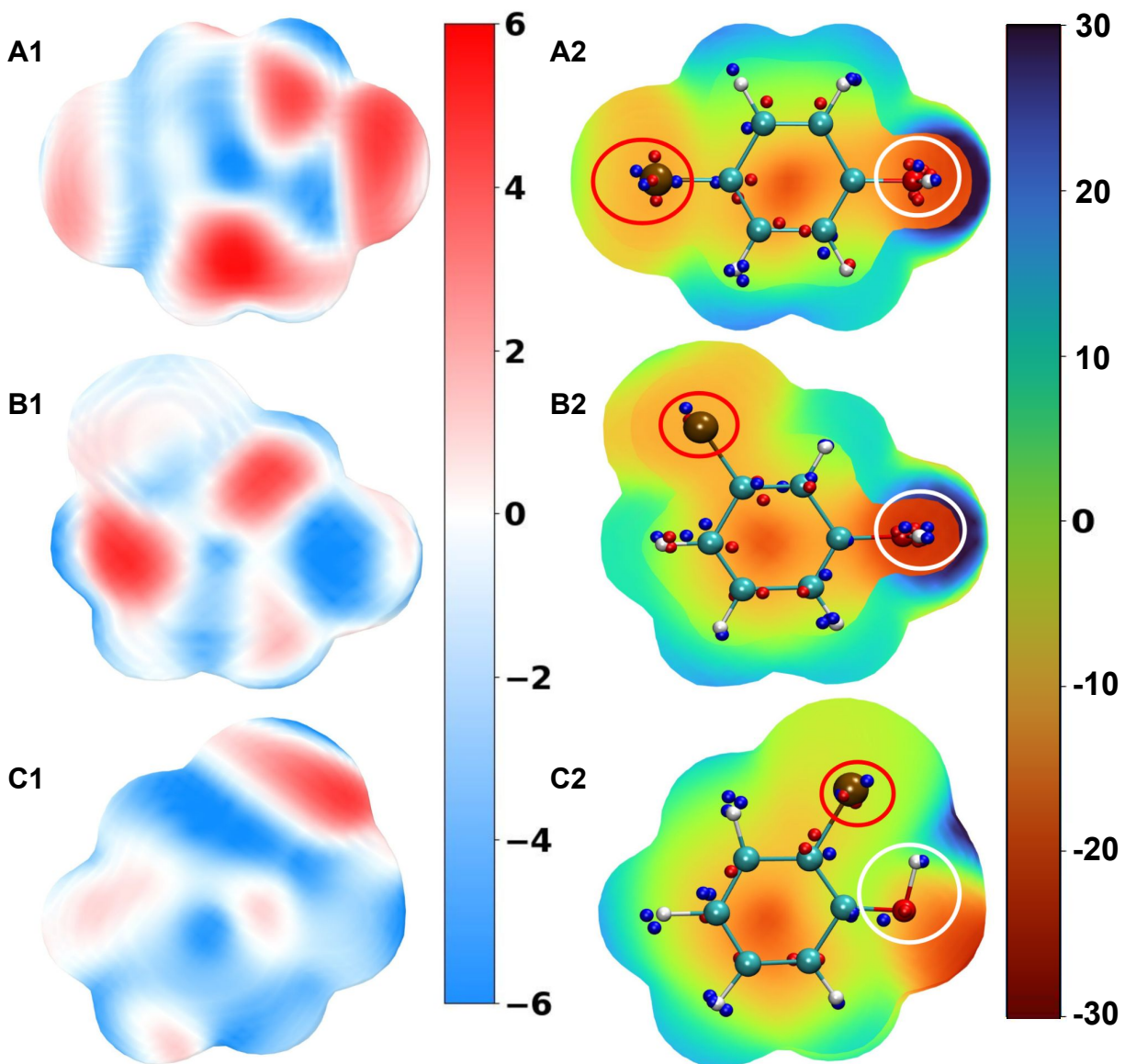


Figure 4: Left column: Difference ESP ( $\Delta$ ESP) between the *ab initio* reference (MP2/aug-cc-pVTZ) and MDCM-generated ESP. Right column: the total ESP from the MDCM models. Results for *p*-, *m*-, and *o*-Cl-PhOH (from top to bottom) are reported on the 0.001 isosurface. In panels A2 to C2 the positions of the positive and negative MDCM charges are reported as small blue and red spheres. The structures used in this Figure corresponds to that for which the RMSD compared with the reference ESP is lowest. The average errors for the close, mid, and long ranges are reported in Table 1.

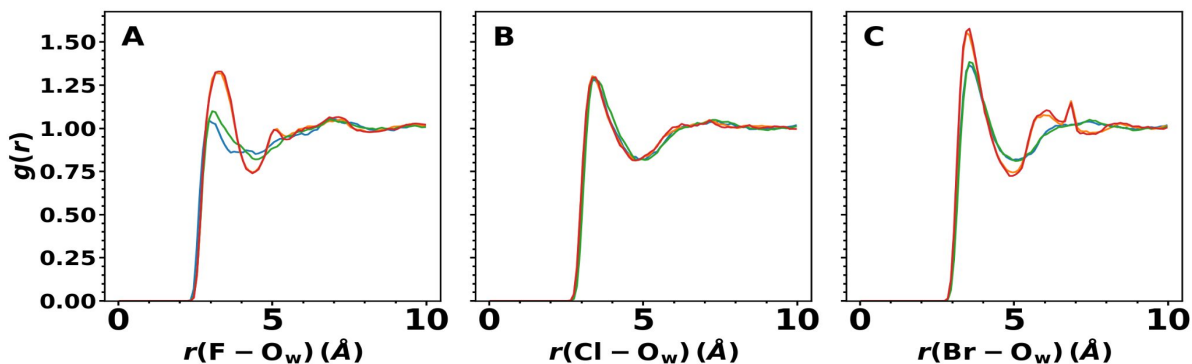


Figure 5: Radial distribution functions  $g_{X-O_w}(r)$  between the halogen and the surrounding water-oxygen atoms for F-Bz, Cl-Bz, and Br-Bz (panels A to C). The blue, orange, green and red traces correspond to simulations using the CGenFF, MDCM, PhysNet and PhysNet+MDCM energy functions. The orange and red traces using the MDCM models are nearly superimposed whereas the atom-centered models (CGenFF and PhysNet) differ slightly for F-Bz but approach one another for Cl-Bz and Br-Bz.

Compared with earlier simulations for X-Bz using MTPs with refitted van der Waals parameters<sup>41</sup> it is found that the increase in occupation for the first solvent shell for F-Bz is consistent with using a refined charge model such as MDCM. Also, the finding that for Cl-Bz the  $g_{Cl-O_w}(r)$  is largely independent of the charge model used is mirrored in the present work and reassuring. Finally, the increase in water occupation in the first shell for Br-Bz compared with F-Bz and Cl-Bz has been reported from simulations using MTPs for Br-Bz.<sup>41</sup> In conclusion, for the X-Bz systems the present findings for the solvent structure is compatible with earlier simulations using atom-centered multipoles on the same systems.

For *p*- and *m*-Cl-PhOH the radial distribution functions  $g_{O_S-H_W}(r)$  and  $g_{H_{OH,S}-O_W}(r)$  were considered, see Figure 6. The water-hydrogen interacting with the oxygen of the PhOH leads to two prominent peaks at  $\sim 1.7$  Å and  $\sim 3.2$  Å for *p*- and *m*-Cl-PhOH using the CGenFF, MDCM and PhysNet+MDCM energy functions, respectively. The positions of the maxima are nearly identical and the maximum intensities differ by less than 10 %. For simulations using the PhysNet model (featuring fluctuating atom-centered point charges) the first peak is

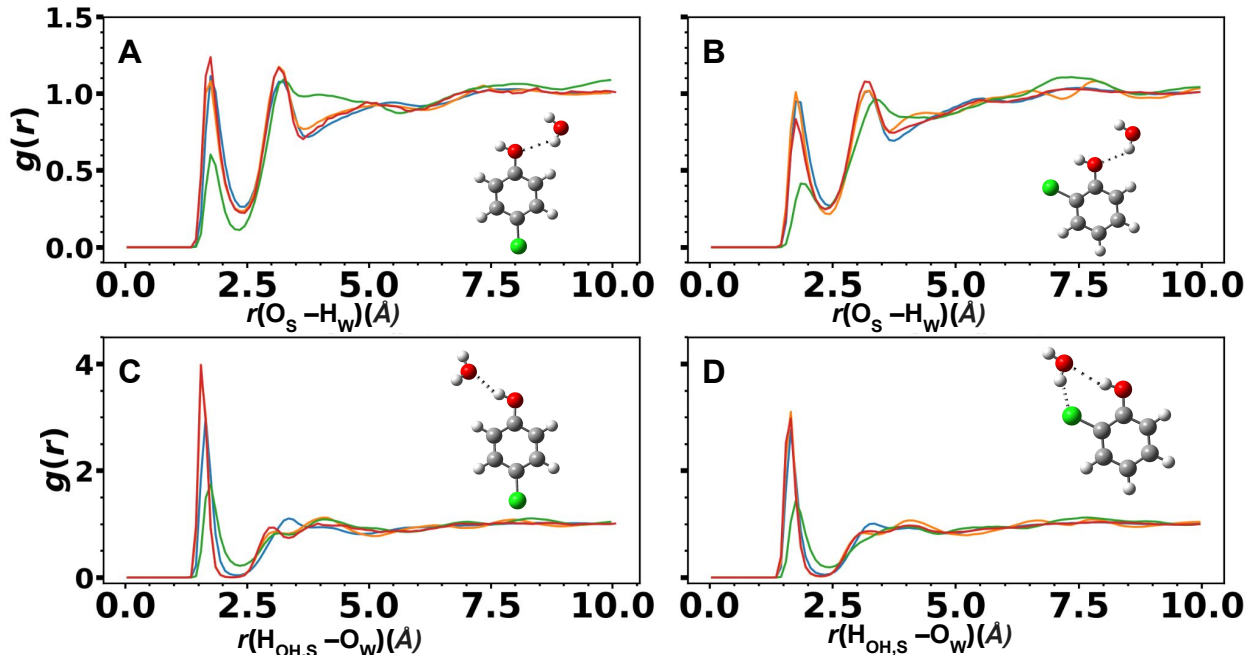


Figure 6: Radial distribution functions between solute (S) and water (W) atoms  $g_{\text{O}_S-\text{H}_W}(r)$  (top) and  $g_{\text{H}_{\text{OH},S}-\text{O}_W}(r)$  (bottom) for *p*-Cl-PhOH (left) and *o*-Cl-PhOH (right). The definition of the atom-atom separations considered is given in the insets in panels A to D. The blue, orange, green and red traces correspond to simulations using the CGenFF, MDCM, PhysNet and PhysNet+MDCM energy functions. For all  $g(r)$  obtained from simulations run with PhysNet the intensity of the first peak is considerably smaller than for the other three models, see also Figure 7.

reduced by  $\sim 50\%$  whereas the second peak has comparable intensity but broadens towards larger separations. A possible rationalization for this is discussed further below. For the hydrogen bond between the hydrogen of the  $\text{PhOH}_{\text{OH}}$  and the water oxygen atoms (Figures 6C and D) simulations using the MDCM models (red and orange traces) yield nearly identical  $g_{\text{O}_{\text{PhOH}}-\text{O}_W}(r)$  whereas those using CGenFF (blue) and PhysNet (green) differ appreciably. This difference is particularly apparent for *p*-Cl-PhOH but less evident for *m*-Cl-PhOH.

To gain further insights into the reasons why PhysNet leads to the observed differences for the first hydration shell (Figure 6), the fluctuating charges from fitting the molecular dipole moments were analyzed, see Figure 7. From 1 ns simulations for *p*-, *m*-, and *o*-Cl-PhOH in solution 50000 structures were extracted in regular intervals. For these structures the dis-

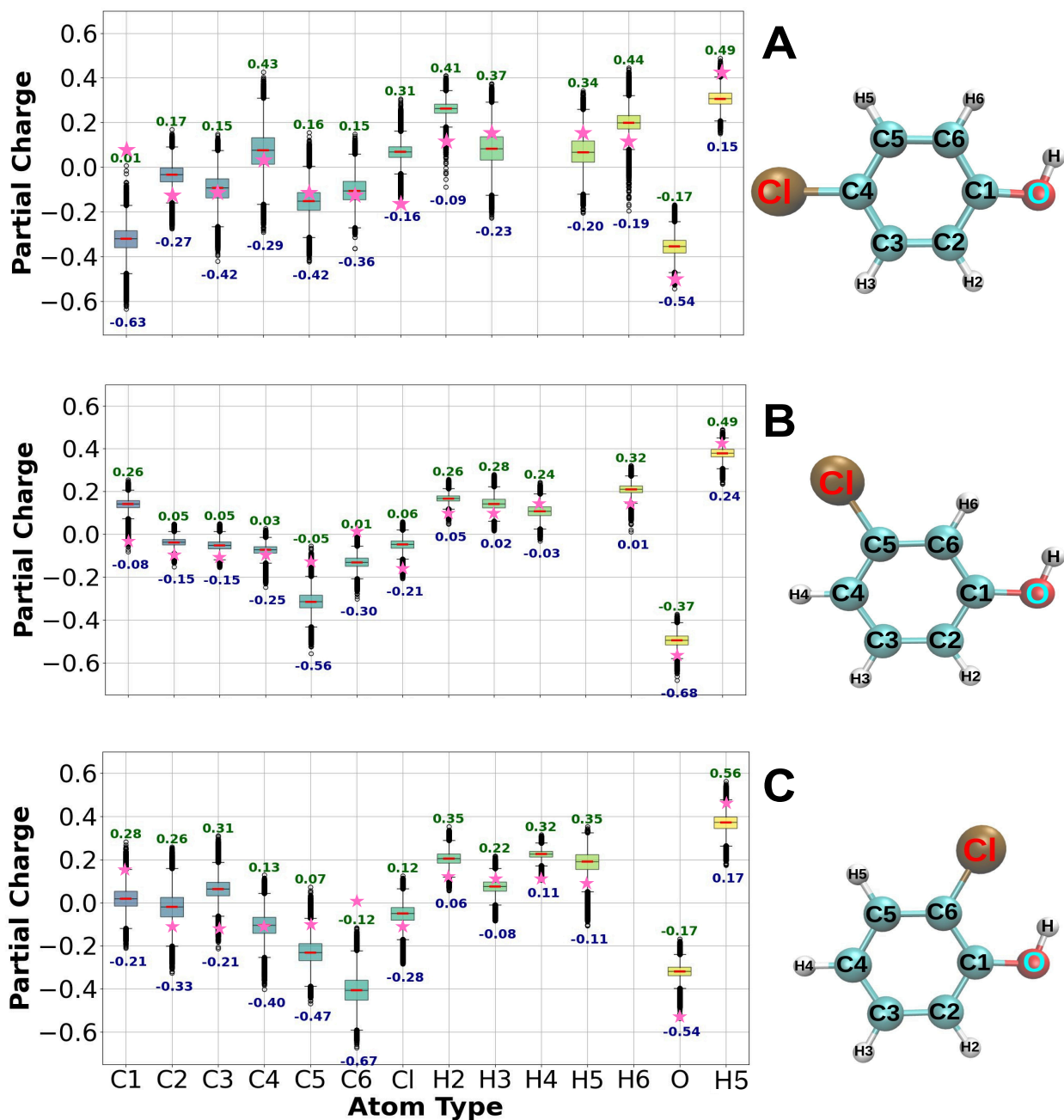


Figure 7: Charge distribution of the conformations for *p*-Cl-PhOH, extracted from the pyCHARMM simulation using PhysNet. For a 1 ns simulation every 10<sup>th</sup> step the geometries for 50000 structures were extracted. The central red line is the median of the charge distribution and the colored region represents the 50 percentile of the charge distribution. The black circles are outliers and the lila stars denote the partial charges from CGenFF. As the Chlorine atom moves from *p*- to *o*- the electronegativity of the associated carbon atom (C-Cl) increases and the electronegativity on C1 or C<sub>α</sub> decreases.

tributions of PhysNet charges were determined, see Figure 7. For *p*-Cl-PhOH the range of  $q_{\text{Cl}}^{\text{PhysNet}}$  spans from  $-0.16e$  to  $+0.31e$  with a 50 percentile of the median (red bar) close to 0. This compares with  $q_{\text{Cl}}^{\text{CGenFF}} = -0.15e$ . Hence, the lowest PhysNet charge is consistent with CGenFF but is larger than the fixed point charge by  $0.16e$ . For *m*-Cl-PhOH and *o*-Cl-PhOH the average  $q_{\text{Cl}}^{\text{PhysNet}}$  shifts progressively towards the value used in CGenFF whereas the span covered in PhysNet remains around  $\sim 0.3e$  to  $\sim 0.4e$ . For the  $\text{O}_{\text{PhOH}}$  the average PhysNet charges for *p*- and *o*-Cl-PhOH (Figures 7A and C) are larger by  $0.15e$  and  $0.20e$ , respectively, than those in CGenFF. Hence, the average interaction energy between  $\text{O}_{\text{PhOH}}$  and the surrounding water is considerably reduced in simulations using PhysNet compared with CGenFF. This rationalizes the reduced occupation of the first solvation shell found in Figure 6.

### 3.4 Infrared Spectroscopy

Infrared spectroscopy is a valuable experimental tool that provides molecular-level information. IR spectra for *p*-Cl-PhOH using the four interaction models are reported in Figure 8. The CH- and OH-stretch-involving vibrations from simulations using CGenFF (panel A) are in good agreement with experiment. This is primarily because the parametrization had been chosen accordingly which is an advantage of empirical energy functions. Using MDCM as the electrostatic model (panel B) shifts the frequencies slightly to the blue whereas the two PhysNet models (panels C and D) lead to more pronounced blue shifts for the CH-stretch whereas the OH-stretch mode is of comparable quality from PhysNet+MDCM (panel D) as CGenFF. The shifts observed for the MDCM model are consistent with earlier work on CO in myoglobin which also reported that multipolar charge distributions shift IR spectra depending on the strengths of the interactions.<sup>20</sup> For the two PhysNet models the differences between simulations and experiments are due to i) the level of theory at which the models were trained and ii) sampling only the bottom of the well in MD simulations which is a

well-understood effect.<sup>70</sup> The pattern of framework modes (below and around 1000  $\text{cm}^{-1}$ ) is realistically captured from CGenFF simulations whereas MDCM widens all bands (panel B). PhysNet in panel C yields a comparably good pattern of vibrations as CGenFF and using PhysNet+MDCM (panel D) broadens the spectral features around 1000  $\text{cm}^{-1}$ . More specifically, the bands at 500  $\text{cm}^{-1}$ , 823  $\text{cm}^{-1}$ , 1176  $\text{cm}^{-1}$ , 1259  $\text{cm}^{-1}$ , 1494, 3073  $\text{cm}^{-1}$  and 3609  $\text{cm}^{-1}$  are well reproduced using CGenFF, whereas the peaks at 644  $\text{cm}^{-1}$  and 1494  $\text{cm}^{-1}$  are less well captured. Comparable observations are made for the simulations using PhysNet. A more detailed analysis and assignments is not attempted here. It is noted that a dedicated experimental/computational study of the vibrational spectroscopy of *p*-F-PhOH showed that the vibrations in the region of the framework modes (1000 to 1200  $\text{cm}^{-1}$  are strongly mixed.<sup>71</sup> Unequivocal assignment of the vibrations was not possible in that case either.

For completeness, computed IR spectra for the X-Benzenes (where X = H, F, Cl, Br) in water are reported in Figure S3 together with available experiments.<sup>73-76</sup> It is noted that data is only available in pure liquids, KBr pellets, or in a liquid film but not in water. Experimentally,<sup>77</sup> four infrared bands were reported for liquid benzene and benzene in the gas phase with center frequencies at  $\sim 675 \text{ cm}^{-1}$ ,  $\sim 1036 \text{ cm}^{-1}$ ,  $\sim 1479 \text{ cm}^{-1}$ , and  $\sim 3070 \text{ cm}^{-1}$ . Using CGenFF (panel A1) for simulations in water these bands are rather well reproduced also because the FF was fitted to do so. Replacing the atom-centered point charges by MDCM widens the absorption band which is consistent with experiments in liquid benzene. With PhysNet (A3) the absorption is shifted to the blue which is a consequence of the level of quantum chemical theory at which the reference data was calculated and the fact that MD simulations sample the bottom of the well.<sup>70</sup> Finally, switching to MDCM charges (A4) again widens the spectrum. For the CH-stretch vibrations a slight blue shift is found for simulations using MDCM (orange) and with PhysNet the shift to the blue is more appreciable. Again, the reasons for these findings are identical to those for Cl-PhOH above. No

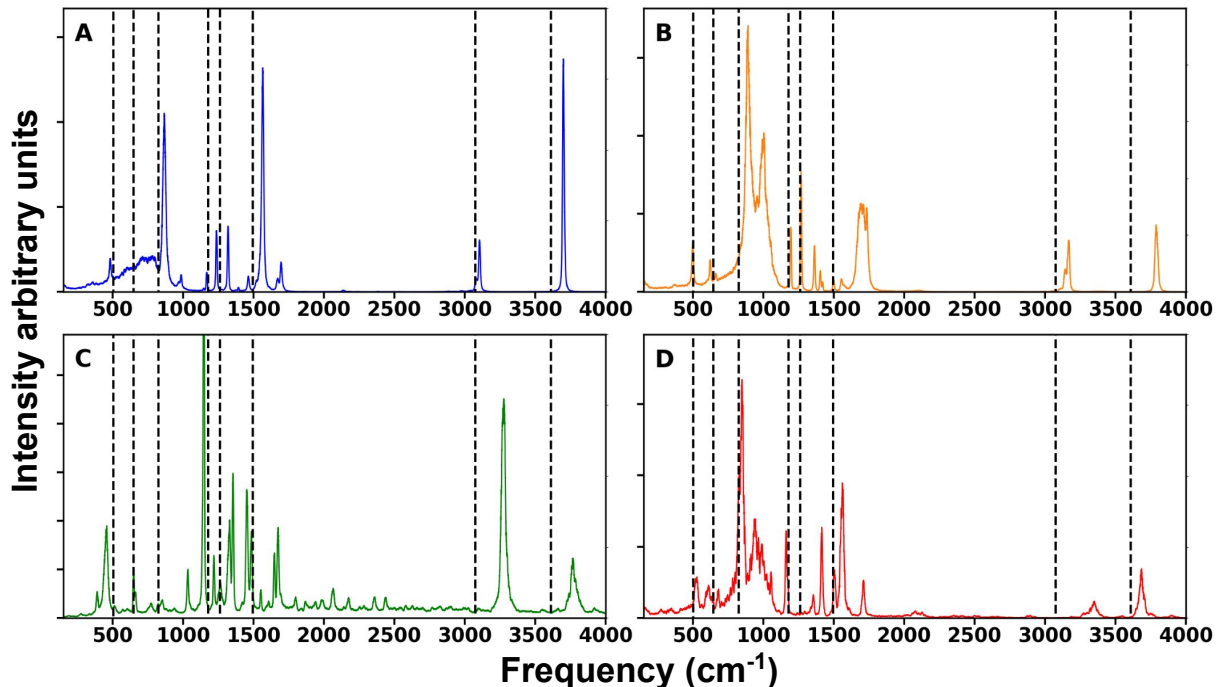


Figure 8: IR spectra for *p*-Cl-PhOH in solvent from MD simulations using the CGenFF, MDCM, PhysNet and PhysNet+MDCM energy functions, panels A to D. The dashed lines indicate the most prominent experimentally measured band maxima which were measured in  $\text{CCl}_4$  and cyclohexane.<sup>72</sup> CGenFF almost exactly reproduces the CH- and OH-stretch frequencies (because the parametrization was chosen accordingly) whereas PhysNet overestimates the frequencies due to sampling only the harmonic well.<sup>70</sup> Also, it is noted that MDCM shifts the CH- and OH-bands somewhat to higher frequencies.

attempt is made for a detailed assignment of the framework modes for halogenated benzenes.

### 3.5 Hydration Free Energies

Finally, hydration free energies from using the CGenFF, MDCM and PhysNet models were determined. For PhysNet+MDCM additional code developments will be required. Using MDCM two different approaches were chosen. In the first the standard CGenFF van der Waals parameters were used whereas in the second the van der Waals ranges were allowed to vary to better reproduce the experimentally observed  $\Delta G_{\text{hyd}}$ . Adaptation of the van der Waals ranges is known to be necessary if the underlying electrostatic model is changed.<sup>4,68,78</sup>

Using the point-charge-based CGenFF parametrization the hydration free energies for all compounds considered are in reasonably good agreement with experiment, see Table 2, except for F-Bz. Typical deviations are 10 % to 25 % and most of the rankings are correctly reproduced. This is to be expected as hydration free energies were part of the parametrization procedure of the energy function.<sup>13,14</sup>

Replacing PCs by MDCMs to capture charge anisotropy but retaining the remaining parameters of the CGenFF energy function overestimates  $\Delta G_{\text{hyd}}$  for X-Bz by about a factor of 2 for halogens and a factor of 6 for benzene, see Table 2. On the other hand, for the three Cl-PhOH species the performance is rather encouraging, in particular for *m*-Cl-PhOH. For *p*- and *o*-Cl-PhOH the hydration free energy is overestimated by about 25 % or  $\sim 2.5$  kcal/mol. As is well known, replacing the electrostatic model in an empirical energy function also requires the van der Waals parameters to be readjusted. Scaling the  $\sigma$ -parameters (range) is one possibility which was followed here. For the X-Bz species, increasing the vdw-ranges by up to 20 % yields satisfactory results - certainly within experimental error bars of  $\sim 1$  kcal/mol - whereas for the Cl-PhOH species scaling by 20 % improves the performance considerably. The only exception is benzene for which increasing the vdw-ranges still leads to an overestimation by a factor of 3. It was already found previously that in addition to modifying  $\sigma$ -values it may also be necessary to decrease the well depth  $\epsilon$  of the van der Waals interactions.<sup>30</sup> In addition, the MDCM models for X-Bz were not conformationally averaged and doing so may further improve the hydration free energies for benzene.

Finally,  $\Delta G_{\text{hyd}}$  were also determined from simulations using PhysNet which is based on fluctuating atom-centered point charges together with van der Waals parameters from CGenFF. Because PhysNet returns only the total energy (bonded plus electrostatics) of the solute and the solute-solvent interactions, scaling of the energies as per Eq. 3 needs to be carried

out differently. Two possibilities were considered in the present work. In the first the total energy of the solute (bonded plus electrostatics) and the solute–solvent interactions were scaled from 0 to 1 following Eq. 3, see Table 2. Secondly, only the solute-solvent interactions were scaled from 0 to 1 but the total energy of the solute was not scaled ( $\lambda = 1$  throughout). The latter approach leads to more favourable binding (more negative  $\Delta G_{\text{hyd}}$ ) by  $\sim 10$  %. This yields qualitatively correct rankings of the hydration free energies. For X-Bz the  $\Delta G_{\text{hyd}}$  are somewhat too uniform for H-, F-, and Cl-Bz but their magnitude is meaningful. Hydration free energies for the three Cl-PhOH molecules are too weak by  $\sim 50$  %. Again, for quantitative hydration free energies the van der Waals parameters will need to be readjusted

Table 2: Hydration free energies  $\Delta G_{\text{hyd}}$  for the different compounds and energy functions considered in the present work. Comparison between point charge model (PC), Minimally distributed charge model (MDCM), and PhysNet. The performances were benchmarked against experimental values.<sup>79–82</sup>  $\Delta G_{\text{hyd}}$  using MDCM were obtained using the same CGenFF Lennard-Jones parameters whereas for  $\Delta G_{\text{hyd}}^*$  the Van der Waals radii were increased by 30 % for H-Bz, by 20 % for *o*-Cl-PhOH and Cl-Bz, and by 10 % for all other molecules. Error bars were determined from averages over 4 independent simulations. Typical experimental errors for neutrals are estimated at  $\sim \pm 1$  kcal/mol.<sup>83</sup>

Molecules	$\Delta G_{\text{hyd}}$ PC	$\Delta G_{\text{hyd}}$ MDCM	$\Delta G_{\text{hyd}}^*$ MDCM	$\Delta G_{\text{hyd}}$ PhysNet	$\Delta G_{\text{hyd}}$ Exp
H-Bz	$-0.91 \pm 0.33$	$-4.90 \pm 0.80$	$-2.69 \pm 0.79$	$-1.21 \pm 0.23$	-0.87
F-Bz	$-1.49 \pm 0.45$	$-1.60 \pm 0.51$	$-1.12 \pm 0.61$	$-1.12 \pm 0.22$	-0.78
Cl-Bz	$-1.14 \pm 0.39$	$-2.91 \pm 0.45$	$-1.75 \pm 0.77$	$-1.22 \pm 0.22$	-1.12
Br-Bz	$-1.58 \pm 0.46$	$-2.65 \pm 0.38$	$-1.96 \pm 0.40$	$-1.30 \pm 0.23$	-1.46
<i>p</i> -Cl-PhOH	$-5.01 \pm 0.74$	$-9.47 \pm 0.81$	$-7.50 \pm 0.81$	$-3.91 \pm 0.42$	-7.03
<i>m</i> -Cl-PhOH	$-6.37 \pm 0.70$	$-6.80 \pm 0.79$	$-6.80 \pm 0.79$	$-3.68 \pm 0.41$	-6.62
<i>o</i> -Cl-PhOH	$-5.85 \pm 0.74$	$-7.20 \pm 0.52$	$-5.02 \pm 0.49$	$-3.01 \pm 0.44$	-4.55

because the charge model was modified. This is akin to replacing point charges in CGenFF by MDCM, see above.

It is of interest to analyze the hydration free energies together with the radial distribution functions. This was done for *p*-Cl-PhOH, see Figure 6C. The height of the first peak  $g_{\text{H}_{\text{OH,S}}-\text{O}_{\text{W}}}(r)$  decreases in magnitude in going from orange/red (overlapping) to blue to green, i.e. MDCM-based, PC, and PhysNet models. The corresponding hydration free energies change from  $-9.5$  to  $-5.0$  to  $-3.9$  kcal/mol. In other words, the hydration free energies decrease in concert with the maximum probability to find a hydration water molecule in the first solvation shell. This is also consistent with the statistical mechanical interpretation of the pair distribution function as the average strength of the pair interaction. Findings for *o*-Cl-PhOH follow related trends when comparing Figure 6D with the data in Table 2.

Overall, all charge models yield correct rankings with MDCM and readjusted van der Waals parameters perform best. For *m*-Cl-PhOH no adjustment was required whereas for *p*- and *o*-Cl-PhOH the ranges need to be scaled by 10 % to obtain agreement with experiment when accounting for measurement errors. It is notable that for benzene using MDCM rather large modifications are needed which indicates that a charge model that includes charge anisotropy is not suitable and also not necessary. This can be understood by noting that for H-Bz an atom centered PC model is expected to suffice for modeling the weak solvent-solute interactions. Introducing a more elaborate MDCM model may better model the ESP but for correct thermodynamic properties (here  $\Delta G_{\text{hyd}}$ ) the van der Waals terms need to compensate any exaggeration in representing the ESP alone. Thus, more elaborate representations of the ESP can lead to models less suitable for condensed-phase simulations because balancing the different terms is challenging. This is consistent with earlier findings for multipole-based approaches.<sup>4,78</sup>

## 4 Conclusions

The present work assesses the possibility and effects of replacing specific contributions to an empirical energy function with either more detailed electrostatics (PC to MDCM) or all bonded terms by a ML-based representation. This was done for halogen-substituted benzenes and chlorinated phenol in the gas phase and in solution. As expected, changes in the electrostatics lead to modified hydration shells as evidenced in pair distribution functions between solutes and water. This also impacts hydration free energies for which modifications in the electrostatics require adaptation of the van der Waals parameters. In particular for the three Cl-PhOH the agreement between experiment and simulations using an MDCM model is encouraging. On the other hand, for benzene (H-Bz) the present MDCM model requires unusually large van der Waals ranges and additional modification of van der Waals  $\epsilon$ -values and/or conformational averaging for the MDCM model may be required for hydration free energies in better agreement with experiments. Fluctuating atom-centered charges as available from PhysNet, on the other hand, yield models that can be easily brought into agreement with experiment by slightly scaling the van der Waals parameters. The IR spectroscopy of Cl-PhOH is quite well captured by all models used whereas for the halogenated benzenes comparison between experiment and simulations is more difficult due to the different environments in which the measurements were carried out.

The available tools to refine empirical energy functions provide a basis for more targeted improvement for specific applications. This is of particular relevance for interpretation and eventually prediction using atomistic simulations. On the other hand, the present work finds that empirical energy functions serve as a good starting point for exploring the structure, dynamics and thermodynamics of hydrated systems. Improving on them requires high levels of electronic structure calculations, depends on the observables considered, and necessitates the analysis and improvement of the entire energy function, and not only parts of it. One point not addressed in the present work relates to the water model used. For consistency with the

CGenFF parametrization, the TIP3P model was used here. Recent work on eutectic liquids investigated changes in the parametrization if another water model is used.<sup>4</sup> However, the performance of the final models was comparable after fitting to the same electronic structure reference data.

## Data Availability

The data accompanying this work is available at <https://github.com/MMunibas/halobenzenes>.

## Acknowledgment

We thank the Swiss National Science Foundation (grants 200020\_219779 and 200021\_215088) (to MM), and the University of Basel for supporting this work.

## References

- (1) Shaw, D. E.; Maragakis, P.; Lindorff-Larsen, K.; Piana, S.; Dror, R. O.; Eastwood, M. P.; Bank, J. A.; Jumper, J. M.; Salmon, J. K.; Shan, Y.; Wriggers, W. Atomic-Level Characterization of the Structural Dynamics of Proteins. Science **2010**, 330, 341–346.
- (2) Devereux, M.; Boittier, E. D.; Meuwly, M. Systematic improvement of empirical energy functions in the era of machine learning. J. Comp. Chem. **2024**,
- (3) Töpfer, K.; Pasti, A.; Das, A.; Salehi, S. M.; Vazquez-Salazar, L. I.; Rohrbach, D.; Feurer, T.; Hamm, P.; Meuwly, M. Structure, Organization, and Heterogeneity of Water-Containing Deep Eutectic Solvents. J. Am. Chem. Soc. **2022**, 144, 14170–14180.

- (4) Töpfer, K.; Boittier, E.; Devereux, M.; Pasti, A.; Hamm, P.; Meuwly, M. Force Fields for Deep Eutectic Mixtures: Application to Structure and 2D-Infrared Spectroscopy. arXiv preprint arXiv:2408.07638 **2024**,
- (5) MacKerell, A. D. et al. All-atom Empirical Potential for Molecular Modeling and Dynamic s Studies of Proteins. J. Phys. Chem. B **1998**, 102, 3586–3616.
- (6) Weiner, S. J.; Kollman, P. A.; Case, D. A.; a nd C. Ghio, U. S.; Alagona, G.; Profeta Jr, S.; Weiner, P. A new force-field for molecular mechanical simulation of nucleic-acids and proteins. J. Am. Chem. Soc. **1984**, 106, 765–784.
- (7) Hermans, J.; Berendsen, H. J. C.; van Gunsteren, W. F.; Postma, J. P. M. A consistent empirical potential for water-protein interactions. Biopol. **1984**, 23, 1513–1518.
- (8) Jorgensen, W. L.; Tirado-Rives, J. The OPLS potential functions for proteins - energy minimization s for crystals of cyclic-peptides and crambin. J. Am. Chem. Soc. **1988**, 110, 1657–1666.
- (9) Huang, J.; Lopes, P. E.; Roux, B.; MacKerell Jr, A. D. Recent advances in polarizable force fields for macromolecules: microsecond simulations of proteins using the classical Drude oscillator model. J. Phys. Chem. Lett. **2014**, 5, 3144–3150.
- (10) Nilsson, L.; Karplus, M. Empirical energy functions for energy minimization and dynamics of nucleic acids. J. Comp. Chem. **1986**, 7, 591–616.
- (11) Price, S. L. Predicting crystal structures of organic compounds. Chem. Soc. Rev. **2014**, 43, 2098–2111.
- (12) Deringer, V. L. Modelling and understanding battery materials with machine-learning-driven atomistic simulations. Journal of Physics: Energy **2020**, 2, 041003.
- (13) Kumar, A.; Yoluk, O.; MacKerell Jr, A. D. FFParm: Standalone package for

- CHARMM additive and Drude polarizable force field parametrization of small molecules. J. Comp. Chem. **2020**, 41, 958–970.
- (14) Kumar, A.; MacKerell Jr, A. D. FFParam-v2. 0: A Comprehensive Tool for CHARMM Additive and Drude Polarizable Force-Field Parameter Optimization and Validation. J. Phys. Chem. B **2024**, 128, 4385–4395.
- (15) Halgren, T. A. Merck molecular force field. I. Basis, form, scope, parameterization, and performance of MMFF94. J. Comp. Chem. **1996**, 17, 490–519.
- (16) Koner, D.; Salehi, S. M.; Mondal, P.; Meuwly, M. Non-conventional force fields for applications in spectroscopy and chemical reaction dynamics. J. Chem. Phys. **2020**, 153.
- (17) Meuwly, M. Atomistic simulations for reactions and vibrational spectroscopy in the era of machine learning - quo vadis? J. Phys. Chem. B **2022**, 126, 2155–2167.
- (18) Unke, O. T.; Meuwly, M. Toolkit for the Construction of Reproducing Kernel-based Representations of Data: Application to Multidimensional Potential Energy Surfaces. J. Chem. Inf. and Mod. **2017**, 57, 1923–1931.
- (19) Käser, S.; Vazquez-Salazar, L. I.; Meuwly, M.; Töpfer, K. Neural network potentials for chemistry: concepts, applications and prospects. Dig. Disc. **2023**, 2, 28–58.
- (20) Nutt, D. R.; Meuwly, M. Theoretical investigation of infrared spectra and pocket dynamics of photodissociated carbonmonoxy myoglobin. Biophys. J. **2003**, 85, 3612–3623.
- (21) Nutt, D. R.; Meuwly, M. CO migration in native and mutant myoglobin: atomistic simulations for the understanding of protein function. Proc. Natl. Acad. Sci. **2004**, 101, 5998–6002.
- (22) Lee, M. W.; Meuwly, M. On the role of nonbonded interactions in vibrational energy relaxation of cyanide in water. J. Phys. Chem. A **2011**, 115, 5053–5061.

- (23) Cazade, P.-A.; Hedin, F.; Xu, Z.-H.; Meuwly, M. Vibrational relaxation and energy migration of N-methylacetamide in water: The role of nonbonded interactions. J. Phys. Chem. B **2015**, 119, 3112–3122.
- (24) Jorgensen, W. L.; Schyman, P. Treatment of halogen bonding in the OPLS-AA force field: application to potent anti-HIV agents. J. Chem. Theo. Comp. **2012**, 8, 3895–3901.
- (25) Stone, A. Distributed multipole analysis, or how to describe a molecular charge distribution. Chem. Phys. Lett. **1981**, 83, 233–239.
- (26) Sokalski, W. A.; Poirier, R. Cumulative atomic multipole representation of the molecular charge distribution and its basis set dependence. Chem. Phys. Lett. **1983**, 98, 86–92.
- (27) Piquemal, J.-P.; Chevreau, H.; Gresh, N. Toward a Separate Reproduction of the Contributions to the Hartree- Fock and DFT Intermolecular Interaction Energies by Polarizable Molecular Mechanics with the SIBFA Potential. J. Chem. Theo. Comp. **2007**, 3, 824–837.
- (28) Shaik, M. S.; Devereux 1, M.; Popelier, P. L. The importance of multipole moments when describing water and hydrated amino acid cluster geometry. Mol. Phys. **2008**, 106, 1495–1510.
- (29) Kramer, C.; Gedeck, P.; Meuwly, M. Atomic multipoles: Electrostatic potential fit, local reference axis systems, and conformational dependence. J. Comp. Chem. **2012**, 33, 1673–1688.
- (30) Bereau, T.; Kramer, C.; Meuwly, M. Leveraging Symmetries of Static Atomic Multipole Electrostatics in Molecular Dynamics Simulations. J. Comp. Chem. **2013**, 9, 5450–5459.
- (31) Price, S. L.; Hamad, S.; Torrisi, A.; Karamertzanis, P.; Leslie, M.; Catlow, C. Applica-

- tions of DL\_POLY and DL\_MULTI to organic molecular crystals. Mol. Sim. **2006**, 32, 985–997.
- (32) Piquemal, J.-P.; Cisneros, G. A.; Reinhardt, P.; Gresh, N.; Darden, T. A. Towards a force field based on density fitting. J. Chem. Phys. **2006**, 124.
- (33) Joubert, L.; Popelier, P. Improved convergence of the ‘atoms in molecules’ multipole expansion of electrostatic interaction. Mol. Phys. **2002**, 100, 3357–3365.
- (34) Devereux, M.; Raghunathan, S.; Fedorov, D. G.; Meuwly, M. A Novel, computationally efficient multipolar model employing distributed charges for molecular dynamics simulations. J. Chem. Theo. Comp. **2014**, 10, 4229–4241.
- (35) Unke, O. T.; Devereux, M.; Meuwly, M. Minimal distributed charges: Multipolar quality at the cost of point charge electrostatics. J. Chem. Phys. **2017**, 147, 161712.
- (36) Devereux, M.; Pezzella, M.; Raghunathan, S.; Meuwly, M. Polarizable Multipolar Molecular Dynamics Using Distributed Point Charges. J. Chem. Theo. Comp. **2020**, 16, 7267–7280.
- (37) Boittier, E. D.; Devereux, M.; Meuwly, M. Molecular Dynamics with Conformationally Dependent, Distributed Charges. J. Chem. Theo. Comp. **2022**, 18, 7544–7554, PMID: 36346403.
- (38) Boittier, E.; Töpfer, K.; Devereux, M.; Meuwly, M. Kernel-Based Minimal Distributed Charges: A Conformationally Dependent ESP-Model for Molecular Simulations. J. Chem. Theo. Comp. **2024**,
- (39) Gao, Q.; Yokojima, S.; Fedorov, D. G.; Kitaura, K.; Sakurai, M.; Nakamura, S. Octahedral point-charge model and its application to fragment molecular orbital calculations of chemical shifts. Chem. Phys. Lett. **2014**, 593, 165–173.

- (40) Clark, T.; Hennemann, M.; Murray, J. S.; Politzer, P. Halogen bonding: The  $\sigma$ -hole: Proceedings of “Modeling interactions in biomolecules II”, Prague, September 5th–9th, 2005. J. Mol. Model. **2007**, 13, 291–296.
- (41) El Hage, K.; Bereau, T.; Jakobsen, S.; Meuwly, M. Impact of quadrupolar electrostatics on atoms adjacent to the sigma-hole in condensed-phase simulations. J. Chem. Theo. Comp. **2016**, 12, 3008–3019.
- (42) Faerman, C. H.; Price, S. L. A transferable distributed multipole model for the electrostatic interactions of peptides and amides. J. Am. Chem. Soc. **1990**, 112, 4915–4926.
- (43) Reynolds, C. A.; Essex, J. W.; Richards, W. G. Atomic charges for variable molecular conformations. J. Am. Chem. Soc. **1992**, 114, 9075–9079.
- (44) Koch, U.; Popelier, P.; Stone, A. Conformational dependence of atomic multipole moments. Chem. Phys. Lett. **1995**, 238, 253–260.
- (45) Plattner, N.; Meuwly, M. The role of higher CO-multipole moments in understanding the dynamics of photodissociated carbonmonoxide in myoglobin. Biophys. J. **2008**, 94, 2505–2515.
- (46) Kim, S. S.; Rhee, Y. M. Modeling Charge Flux by Interpolating Atomic Partial Charges. J. Chem. Inf. and Mod. **2019**, 59, 2837–2849.
- (47) Upadhyay, M.; Meuwly, M. CO<sub>2</sub> and NO<sub>2</sub> formation on amorphous solid water. Astron. Astrophys. **2024**, 689, A319.
- (48) Brooks, B. R. et al. CHARMM: The Biomolecular Simulation Program. J. Comp. Chem. **2009**, 30, 1545–1614.
- (49) Hwang, W. et al. CHARMM at 45: Enhancements in Accessibility, Functionality, and Speed. J. Phys. Chem. B **2024**, in print, null.

- (50) Unke, O. T.; Meuwly, M. PhysNet: A Neural Network for Predicting Energies, Forces, Dipole Moments, and Partial Charges. J. Chem. Theo. Comp. **2019**, 15, 3678–3693.
- (51) Song, K.; Käser, S.; Töpfer, K.; Vazquez-Salazar, L. I.; Meuwly, M. PhysNet meets CHARMM: A framework for routine machine learning/molecular mechanics simulations. J. Chem. Phys. **2023**, 159.
- (52) Buckner, J.; Liu, X.; Chakravorty, A.; Wu, Y.; Cervantes, L. F.; Lai, T. T.; Brooks, C. L. I. pyCHARMM: Embedding CHARMM Functionality in a Python Framework. J. Chem. Theo. Comp. **2023**, 19, 3752–3762.
- (53) Jorgensen, W. L.; Chandrasekhar, J.; Madura, J. D.; Impey, R. W.; Klein, M. L. Comparison of simple potential functions for simulating liquid water. J. Chem. Phys. **1983**, 79, 926–935.
- (54) Ryckaert, J.-P.; Ciccotti, G.; Berendsen, H. J. C. . Numerical integration of the cartesian equations of motion of a system with constraints: molecular dynamics of n-alkanes. J. Chem. Phys. **1977**, 23, 327–341.
- (55) Frisch, M. J. et al. Gaussian~16 Revision C.01. 2016; Gaussian Inc. Wallingford CT.
- (56) Storn, R.; Price, K. Differential Evolution – A Simple and Efficient Heuristic for global Optimization over Continuous Spaces. J. Glob. Optim. **1997**, 11, 341–359.
- (57) Gilmer, J.; Schoenholz, S. S.; Riley, P. F.; Vinyals, O.; Dahl, G. E. Neural Message Passing for Quantum Chemistry. Proceedings of the 34th International Conference on Machine Learning. 2017; pp 1263–1272.
- (58) Scarselli, F.; Gori, M.; Tsoi, A. C.; Hagenbuchner, M.; Monfardini, G. The graph neural network model. IEEE Trans. Neural Netw. Learn. Syst. **2008**, 20, 61–80.
- (59) Kingma, D. P. Adam: A method for stochastic optimization. arXiv preprint arXiv:1412.6980 **2014**,

- (60) Reddi, S. J.; Kale, S.; Kumar, S. On the convergence of adam and beyond. arXiv preprint arXiv:1904.09237 **2019**,
- (61) Bannwarth, C.; Ehlert, S.; Grimme, S. GFN2-xTB—An Accurate and Broadly Parametrized Self-Consistent Tight-Binding Quantum Chemical Method with Multipole Electrostatics and Density-Dependent Dispersion Contributions. J. Chem. Theo. Comp. **2019**, 15, 1652–1671.
- (62) Larsen, A. H.; Mortensen, J. J.; Blomqvist, J.; Castelli, I. E.; Christensen, R.; Dułak, M.; Friis, J.; Groves, M. N.; Hammer, B.; Hargus, C., et al. The atomic simulation environment—a Python library for working with atoms. J. Phys. Condens. Matter **2017**, 29, 273002.
- (63) Werner, H.-J. et al. The Molpro quantum chemistry package. J. Chem. Phys. **2020**, 152, 144107.
- (64) Michaud-Agrawal, N.; Denning, E. J.; Woolf, T. B.; Beckstein, O. MDAnalysis: A toolkit for the analysis of molecular dynamics simulations. J. Comp. Chem. **2011**, 32, 2319–2327.
- (65) Gowers, R. J.; Linke, M.; Barnoud, J.; Reddy, T. J. E.; Melo, M. N.; Seyler, S. L.; Domanski, J.; Dotson, D. L.; Buchoux, S.; Kenney, I. M.; Beckstein, O. MDAnalysis: A Python Package for the Rapid Analysis of Molecular Dynamics Simulations. **2019**,
- (66) Kumar, P.; Marx, D. Quantum corrections to classical time-correlation functions: Hydrogen bonding and anharmonic floppy modes. J. Chem. Phys. **2004**, 121, 9.
- (67) Straatsma, T.; Berendsen, H. Free energy of ionic hydration: Analysis of a thermodynamic integration technique to evaluate free energy differences by molecular dynamics simulations. J. Chem. Phys. **1988**, 89, 5876–5886.

- (68) Lee, M. W.; Carr, J. K.; Göllner, M.; Hamm, P.; Meuwly, M. 2D IR spectra of cyanide in water investigated by molecular dynamics simulations. J. Chem. Phys. **2013**, 139, 054506.
- (69) Bondi, A. van der Waals Volumes and Radii. J. Phys. Chem. **1964**, 68, 441–451.
- (70) Nejad, A.; Suhm, M. A. Concerted pair motion due to double hydrogen bonding: The formic acid dimer case. J. Indian Inst. Sci. **2020**, 100, 5–19.
- (71) Salehi, S. M.; Käser, S.; Töpfer, K.; Diamantis, P.; Pfister, R.; Hamm, P.; Rothlisberger, U.; Meuwly, M. Hydration dynamics and IR spectroscopy of 4-fluorophenol. Phys. Chem. Chem. Phys. **2022**, 24, 26046–26060.
- (72) Zierkiewicz, W.; Michalska, D.; Zeegers-Huyskens, T. Molecular Structures and Infrared Spectra of p-Chlorophenol and p-Bromophenol. Theoretical and Experimental Studies. J. Phys. Chem. A **2000**, 104, 11685–11692.
- (73) Coates, J. Encyclopedia of Analytical Chemistry; John Wiley & Sons, Ltd, 2006.
- (74) Ramasamy, R. FTIR and FT-RAMAN Spectral Investigation of Fluorobenzene. Int. J. Phys. Appl. **2014**, 6, 1–6.
- (75) Uno, T.; Kuwae, A.; Machida, K. Vibrational spectra of bromobenzene-4-d1 and bromobenzene-2,3,5,6-d4 and force field of bromobenzene. Spectrochim. Acta A **1977**, 33, 607–614.
- (76) Zhou, Z.-Y.; Kang, X.; Song, Y.; Chen, S. Enhancement of the electrocatalytic activity of Pt nanoparticles in oxygen reduction by chlorophenyl functionalization. Chem. Commun. **2012**, 48, 3391–3393.
- (77) Bertie, J. E.; Keefe, C. D. Comparison of infrared absorption intensities of benzene in the liquid and gas phases. J. Chem. Phys. **1994**, 101, 4610–4616.

- (78) Lee, M. W.; Meuwly, M. Hydration free energies of cyanide and hydroxide ions from molecular dynamics simulations with accurate force fields. Phys. Chem. Chem. Phys. **2013**, 15, 20303–20312.
- (79) Marenich, A. V.; Kelly, C. P.; Thompson, J. D.; Hawkins, G. D.; Chambers, C. C.; Giesen, D. J.; Winget, P.; Cramer, C. J.; Truhlar, D. G. Minnesota Solvation Database (MNSOL) version 2012. 2020; Retrieved from the Data Repository for the University of Minnesota (DRUM).
- (80) Abraham, M. H.; Whiting, G. S.; Fuchs, R.; Chambers, E. J. Thermodynamics of solute transfer from water to hexadecane. J. Chem. Soc., Perkin Trans. 2 **1990**, 291–300.
- (81) Rizzo, R. C.; Aynechi, T.; Case, D. A.; Kuntz, I. D. Estimation of absolute free energies of hydration using continuum methods: accuracy of partial charge models and optimization of nonpolar contributions. J. Chem. Theo. Comp. **2006**, 2, 128–139.
- (82) Vyboishchikov, S. F.; Voityuk, A. A. Solvation free energies for aqueous and nonaqueous solutions computed using PM7 atomic charges. J. Chem. Inf. and Mod. **2021**, 61, 4544–4553.
- (83) Mobley, D. L.; Guthrie, J. P. FreeSolv: a database of experimental and calculated hydration free energies, with input files. J. Comp. Aid. Mol. Des. **2014**, 28, 711–720.

**SUPPORTING INFORMATION: Machine Learning-Based Enhancements of Empirical Energy Functions: Structure, Dynamics and Spectroscopy of Modified Benzenes**

**S1 PhysNet Models for X-Bz**

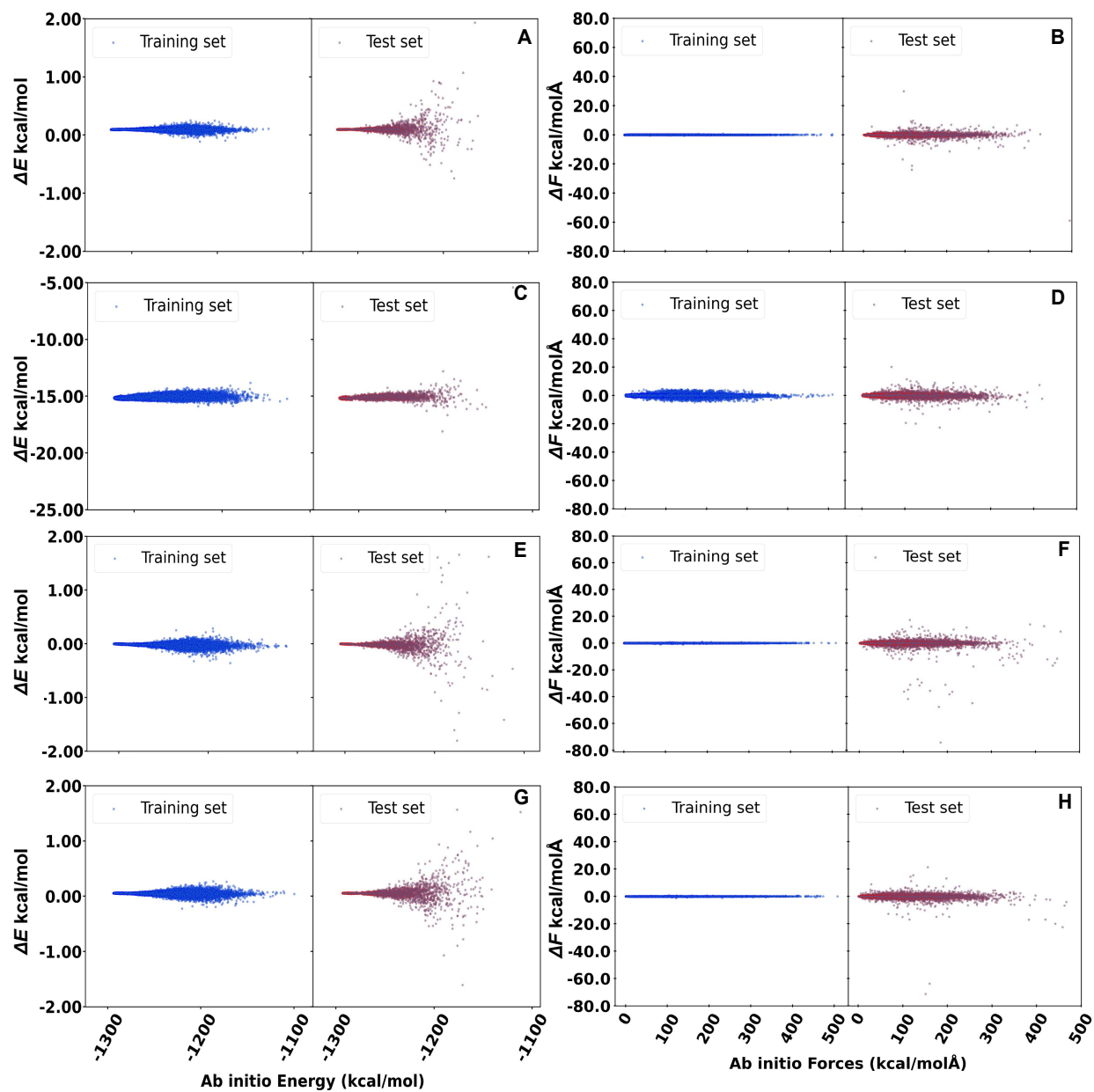


Figure S1: Test set error of PhysNet prediction and reference MP2/6-31G(d,p) calculations for energies (panels A, C, E, G) and forces (B, D, F, H) for X-Bz (X = H, F, Cl, Br) from top to bottom.

## S2 Normal Modes for Cl-PhOH

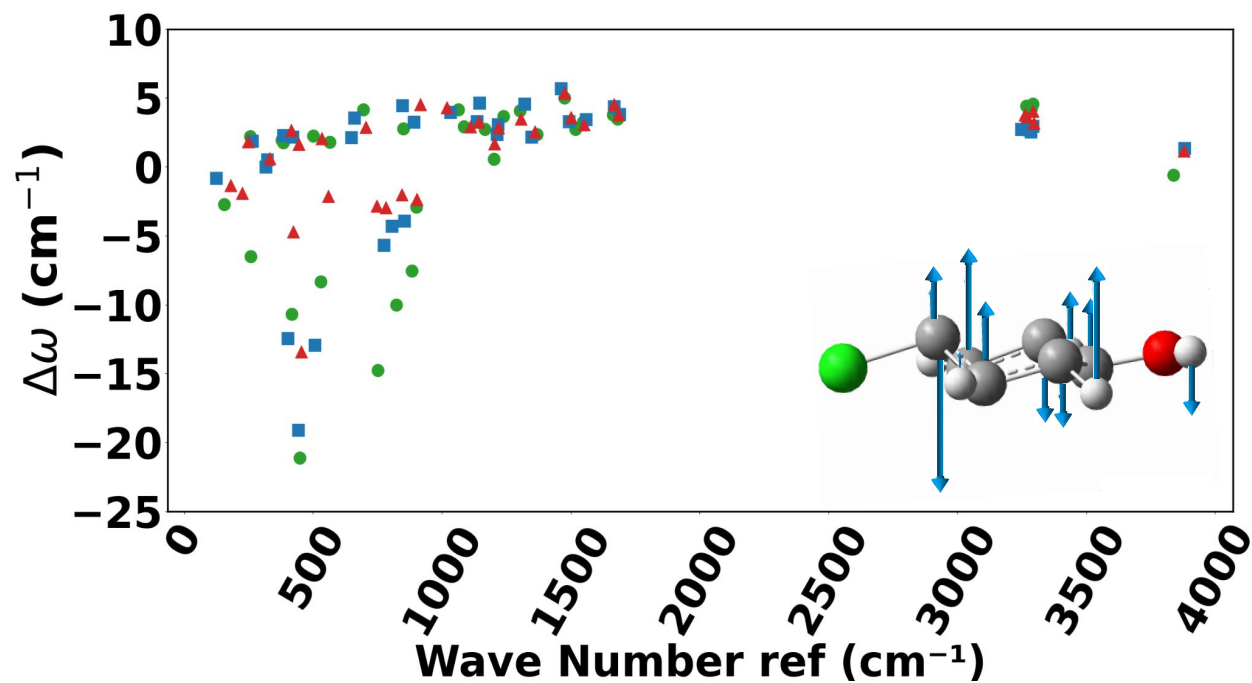


Figure S2: Normal mode analysis for *p*-, *m*-, and *o*-ClPhOH (blue, red, green symbols). The performance of the trained PhysNet model in terms of the difference  $\Delta\omega = \omega_{\text{ref.}} - \omega_{\text{NN}}$  between the *ab initio* reference and that from PhysNet is reported depending on the reference frequency. The inset reports the normal mode vibration with the largest error.

### S3 Infrared Spectroscopy of X-Bz

Figure S3 reports the calculated IR spectra for the X-Benzenes (where X = H, F, Cl, Br) in water with available experiments.<sup>73-76</sup> The IR spectrum for H-Bz is shown in Figure S3A using the CGenFF, MDCM, PhysNet and PhysNet+MDCM energy functions. The influence of the MDCM charges when using the same bonded parameters (CGenFF) is clearly visible in panels A1 and A2. The absorption frequencies remain largely unchanged whereas the intensities clearly depend on the charge model used. For PhysNet with fluctuating and MDCM charges similar effects are found: using atom-centered fluctuating charges (A3) the IR spectrum is comparatively simple whereas replacing them with MDCM charges the positions of the absorptions remain but the intensities redistribute. Experimentally,<sup>77</sup> four infrared bands were reported for liquid benzene and benzene in the gas phase with center frequencies at  $\sim 675\text{ cm}^{-1}$ ,  $\sim 1036\text{ cm}^{-1}$ ,  $\sim 1479\text{ cm}^{-1}$ , and  $\sim 3070\text{ cm}^{-1}$ . Using CGenFF (panel A1) for simulations in water these bands are rather well reproduced also because the FF was fitted to do so. Replacing the atom-centered point charges by MDCM widens the absorption band which is consistent with experiments in liquid benzene. With PhysNet (A3) the absorption is shifted to the blue which is a consequence of the level of quantum chemical theory at which the reference data was calculated and the fact that MD simulations sample the bottom of the well.<sup>70</sup> Finally, switching to MDCM charges (A4) again widens the spectrum. For the modes at lower frequency, similar observations are made.

For the halogenated benzenes in panels B to D the CH-stretch modes behave in the same fashion as for H-Bz. Comparisons for the framework modes between  $500\text{ cm}^{-1}$  and  $1500\text{ cm}^{-1}$  are more difficult because no experimental data for the species in water are available. In general it is noted that the computations yield a larger number of spectroscopic features than the experiments. At this stage a rigorous comparison of experimentally measured spectra for F-, Cl-, and Br-Bz in water is not attempted.

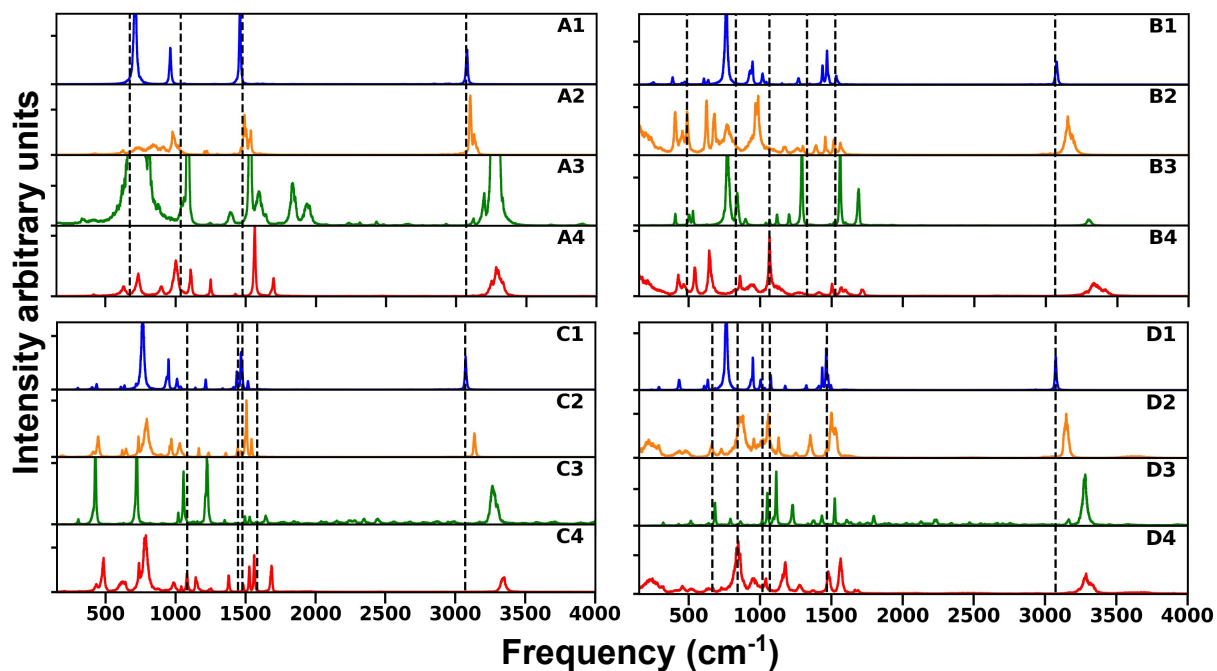


Figure S3: IR spectra for X-Bz in water using the CGenFF, MDCM, PhysNet, and PhysNet+MDCM energy functions (blue, orange, green red). Panels A to D are for H-Bz, F-Bz, Cl-Bz, and Br-Bz, respectively. The black dashed lines are positions of the most prominent lines from the experimental IR spectra which were recorded in the pure liquid (A), in solid KBr pellets (B), in the liquid (C), and in a liquid film (D).<sup>73-76</sup>